

THE NGC 5128 GLOBULAR CLUSTER SYSTEM: A COMPLETE ANALYSIS OF IMAGES USING COSMOS¹

HUGH C. HARRIS

Department of Physics, McMaster University

GRETCHEN L. H. HARRIS

Department of Physics, University of Waterloo

JAMES E. HESSER²

Dominion Astrophysical Observatory, Herzberg Institute of Astrophysics

AND

HARVEY T. MACGILLIVRAY

Royal Observatory, Edinburgh

Received 1984 March 23; accepted 1984 June 20

ABSTRACT

A large region around the peculiar elliptical galaxy NGC 5128 (Centaurus A) has been analyzed using prime focus plates taken in four colors to search for globular clusters. The plates have been scanned with COSMOS and processed to detect and analyze all images (7656 images in the region studied). Image counts show a significant excess of images above background to limiting magnitudes in the range $V = 19-20$, and these results are important for measuring the cluster luminosity function. Nonstellar images are identified, and a visual classification is used to obtain a sample of likely cluster candidates. Their sizes are estimated using a model of the plate-scanner system, and the completeness of the sample is discussed. Most bright clusters have probably been found, so the bright tail of the luminosity function is now fairly well known. The fainter clusters found here are systematically smaller than the brightest, and the sample is probably very incomplete for faint, compact clusters. Therefore the difference in sizes between bright and faint clusters is probably real. In most respects, the cluster system of NGC 5128 appears to be normal for a large elliptical galaxy.

Subject headings: clusters: globular — galaxies: individual

I. INTRODUCTION

Large systems of globular clusters have been identified and studied in numerous elliptical galaxies in the Virgo Cluster (e.g., Hanes 1977; Harris and van den Bergh 1981). Comparison with the smaller cluster systems in the Local Group spirals and dwarf ellipticals is necessary to investigate the "universal" nature of the properties of globular cluster systems. NGC 5128 (Cen A) is the nearest large elliptical galaxy. As such, it provides a unique opportunity to study in detail the properties of a large system of globular clusters. The peculiarities of N5128 are, in one view, only transient (Tubbs 1980; Ebneter and Balick 1983) and are not likely to have significantly influenced the cluster system outside of the dust lane. Indeed, the generally normal nature of the cluster system that is emerging provides support (albeit somewhat circular) for the idea that the spheroid of N5128 is representative of a normal elliptical galaxy.

The proximity of N5128 has already allowed progress in identifying some clusters, confirming membership, and measuring colors and approximate sizes (Graham and Phillips 1980; Frogel 1984; and the present series of papers: van den Bergh, Hesser, and G. Harris 1981; Hesser, *et al.* 1984; Harris *et al.* 1984, hereafter BHH, HHHB, and HHHHC, respectively) to an extent not yet possible in the Virgo Cluster galaxies. However,

progress has been hindered by the severe contamination of the field by foreground stars: the low galactic latitude of N5128 (19°) makes star densities 3 times higher than in Virgo fields, and its proximity also causes the cluster system to be spread over a larger angular extent, reducing the simple detectability (HHBH; Harris 1983). To find the total number of clusters, exhaustive star counts have been carried out by BHH, HHHB, and HHHHC. Clearly, automated techniques for counting images could usefully supplement the manual star counts in the N5128 field. Furthermore, the problem of distinguishing cluster images from foreground stars and background galaxies was discussed by HHHB, who emphasized that their analysis of the cluster properties might be biased by their selection of only the largest clusters. The extent of such selection effects could be examined by using an automated analysis to make objective estimates of the sizes of all objects in the field.

This paper discusses scans of four prime-focus plates made with the COSMOS Facility, Royal Observatory, Edinburgh, and demonstrates some of the achievements that are possible only through an automated approach to image analysis. Image counts are carried out to two intermediate limiting magnitudes ($V_{\text{lim}} = 19-20$). The results are combined with other data by HHHHC to demonstrate that the luminosity function of globular clusters in N5128 is consistent with the luminosity function found for clusters in the Local Group. The size distribution of clusters is analyzed and compared with the size distribution in the Galaxy and M31. Finally, properties of the brightest clusters (more luminous than any in the Galaxy, for any reasonable assumed distance) are discussed and compared with the bulk of less luminous clusters.

¹ Contributions of University of Waterloo Observatory No. xxx.

² Visiting Astronomer, Cerro Tololo Inter-American Observatory, which is operated by the Association of Universities for Research in Astronomy, Inc., under contract with the National Science Foundation.

TABLE 1
PLATES SCANNED BY COSMOS

Plate	Date	Observer	Exposure	Emulsion	Filter	m_{lim}
P5208	81 Mar 11	R. Humphreys	20	IIa-O	GG385	22.5
P5236	81 Apr 1	J. Hesser	15	IIa-D	GG495	22.2
P5719	82 Mar 19	D. McElroy	40	IIIa-F	RG610	22.0
P5727	82 Mar 20	D. McElroy	60	IIIa-J	GG385	23.

II. THE COSMOS SCANS AND REDUCTION PROCEDURES

Two plate pairs, taken in good seeing and each pair having a similar limiting magnitude, were selected for this study. The plates were all taken at the prime focus of the 4 m telescope at the Cerro Tololo Inter-American Observatory. They are listed in Table 1. Three plates were lent to us by Dr. R. Humphreys, to whom we are most grateful. The plates were scanned with COSMOS in 1982 August. Image-detection was completed in Edinburgh in early 1983, and subsequent processing was done at McMaster. Several steps were necessary to ensure uniform detection and measurement of images over the entire usable field of the plates. We describe these steps in the remainder of this section.

Each plate was raster-scanned (using COSMOS mapping mode) over an area 18×18 cm, with a $16 \mu\text{m}$ (0.3) spot size and a $16 \mu\text{m}$ step size. The sensitometer spots on each plate were also scanned for conversion of transmission to intensity. (The spots on each plate were satisfactory in covering the range of density from sky to nearly saturation.) The first step was to smooth the data, replacing each pixel by the mean intensity of the 3×3 pixel box at that position. This smoothing was found not to degrade the resolution noticeably. A correction was then applied to all intensities to account for the radial field distortion produced by the triplet corrector in the prime focus camera. The intensities were increased by a factor of $\Delta A + 1$ (as defined by Chiu 1976) in order that the detection of images would be carried out at the same threshold over the entire field.³

The background (night sky plus halo light of N5128) was then subtracted as follows. A reduced frame was generated for each plate by inserting for each pixel the mean intensity of the corresponding 22×22 (6.5×6.5) pixel region of the original frame. Each reduced frame was filtered using three passes of a two-dimensional median filter, using a different scale length on each pass (scale lengths of 13, 9, and 5 reduced pixels). The filtering effectively removes all stars from the frame, but leaves the halo light intact because of its much larger scale length. A full-size background frame was then generated from the reduced frame by interpolation. Subtraction of the background intensity then left a frame with a flat background having only small-scale features—stars, clusters, background galaxies, and small plate flaws. Only near the dust lane, where the N5128 background is highly irregular, was this procedure not effective.

The COSMOS image-analysis software was then run on the

flattened frame for each plate. The procedure is described fully in the useful publication by Stobie (1982). All pixels above a threshold intensity are grouped into images; the images with areas above a threshold (chosen here to be 20 pixels, or 1.8 arcsec^2) are measured and recorded. Of the various data recorded for each image, we found the position, magnitude, area, major- and minor-axis lengths, orientation, and background were all useful during the subsequent analysis. From 12,600 to 18,100 images were detected on each plate; but, because of the thresholds chosen, the detection limit is not as faint as the plate limit on any of the plates. The last COSMOS process was the merging of the data sets from the four plates. This was done by transforming the positions from three plates to P5236 and finding coincidences. All objects in common on P5208 and P5236 were retained; in practice these were 83% of the images detected on P5236 (the least deep plate), while most plate flaws and Pickering-Racine-prism secondary images were eliminated.

Two final transformations were applied to the data before analysis. First, corrections were made to all images as functions of position on each plate for the effects of field distortions introduced by the triplet corrector. For each image, the position was corrected by Δr , the area made smaller by ΔA , the axis lengths made smaller by ΔS , and the magnitude⁴ made fainter by $-2.5 \log(\Delta A + 1)$, according to the formulae derived by Chiu (1976). Second, the magnitudes were transformed to B , V , J , and F magnitudes using calibration curves for each plate. These were constructed from the photoelectric sequences of Graham (1981) and McElroy and Humphreys (1982), including the Pickering-Racine-prism secondary images of the sequence stars, and eight secondary standards set up using PDS scans of three plates described by HHBH. Following HHBH, a value of $\Delta m = 6.95$ between primary and secondary images was used; therefore, the magnitudes derived in this paper should be on the same system as those in HHBH, and are subject to the same possible systematic errors. We have no reason to believe that systematic errors larger than about 0.1 mag are present for stellar images, but for nonstellar images the magnitudes measured by COSMOS are more complicated (see § IV).

In the region of the dust lane, image detection is not reliable because of the irregular background. Toward the edges of the field, the images are increasingly distorted by coma. Therefore, we have studied only the region shown in Figure 1 (Plate 3). A total of 7656 images were detected in this region.

III. IMAGE COUNTS AND THE NUMBER OF GLOBULAR CLUSTERS

The luminosity function of all images detected in our region of study is shown in Figure 2. The sample is nearly complete to

³ Ordinarily, image detection done at some fractional threshold above local sky is adequate, and no correction is necessary. Here, however, the background light of N5128 must also be subtracted, requiring that field distortion be dealt with separately. Our procedure achieves uniform detection if the field-distortion formulae of Chiu are correct. These formulae were derived for the Kitt Peak 4 m telescope, but they should also apply to our CTIO plates, because both cameras use the same design. Our procedure achieves uniform detection if scattered light is also contributing to the background.

⁴ Ordinarily, no correction to the magnitude *as originally measured* would have been necessary, because the sum of intensity above background is not changed by field distortion. However, because we scaled up the intensities earlier to achieve a uniform detection threshold, we must now scale the magnitudes back down.

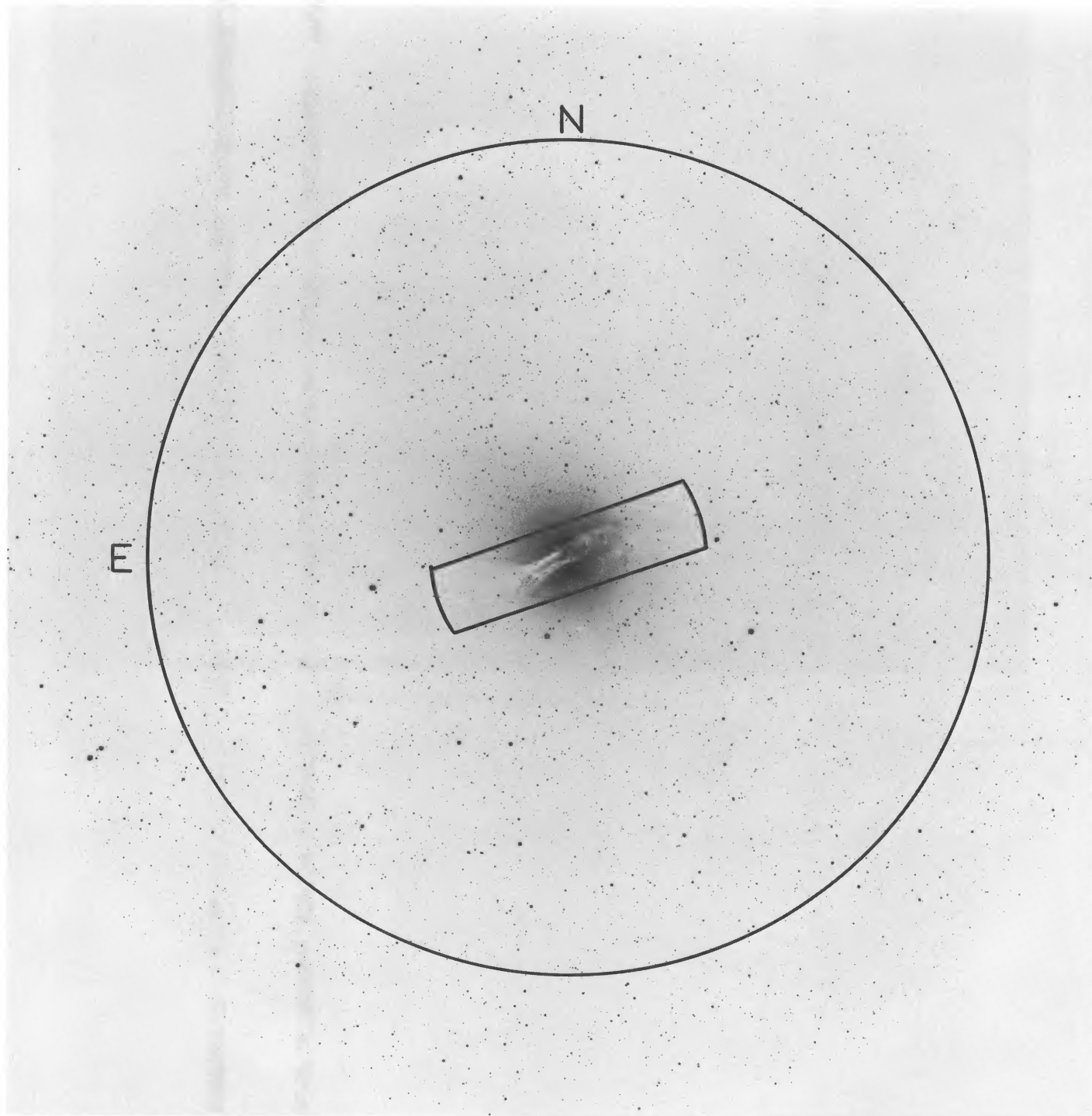


FIG. 1.—Region studied with the COSMOS scans

HARRIS *et al.* (see page 186)

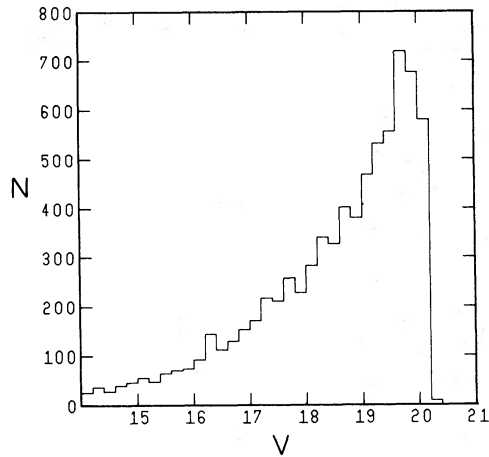


FIG. 2.—Differential luminosity function of all 7656 images detected in our region of study.

a limit $V \sim 20.0$. The V plate is shallower than the others and limits the detection of all but very red objects, and the color-magnitude diagram shown in Figure 3 demonstrates that the limit is nearly independent of color. (Only 1000 images have been plotted in Figure 3 for clarity. In this and subsequent plots of 1000 images, they are the images lying in a strip running through the center of the COSMOS region from north to south.) The cutoff in detected images near $V = 20.0$ is quite sharp because it is well above the plate limit where plate noise is still not large. Fainter images have been found, but have fallen below the image-area threshold of 20 pixels and have been rejected. We should note that extended images (mainly galaxies) near the detection limit have systematically smaller areas, so are only detected to a limiting magnitude somewhat brighter (about 0.2–0.3) mag brighter for galaxies—see the model described in § IV). At this low galactic latitude, however, number counts of galaxies (e.g., Jarvis and Tyson 1981) indi-

cate that galaxies should comprise only about 7% of the images detected at $V = 20$.

Many partially blended objects are detected as one image on one or more plates. Most of these can be identified by their pronounced ellipticity, $e = 1 - b/a$, where a and b (the semi-major and semiminor axes) are recorded from the COSMOS measured moments. The ellipticity found on plate P5236 is shown in Figure 4; similar plots were found for the other plates. For each plate a limit was set (at roughly three times the rms ellipticity for stars). Images lying above these limits on three or four of the plates were assumed to be genuinely elliptical,⁵ and they were flagged as such. Images lying above these limits on only one or two plates (usually due to blending or plate flaws on only one or two plates) were considered round, but only those magnitudes, colors, and sizes measured from the plates where they did *not* appear elliptical were retained.

The region studied in this paper extended from 6 to 72 mm from the center of N5128 on our plates after correction for field distortion, or 1:86–22:31 on the sky. (In the region from 6 to 24 mm, part of the area has been omitted because of the dust lane.) We have divided the region into 22 rings, each 3 mm in width, and treated the number of objects in each ring as is usually done in visual star counts. We have used the region from 51 to 72 mm (15:80–22:31) to estimate the density of background objects. This choice agrees most closely with Case 2 used by HHHC, and it is a good compromise between using a greater background region to improve the statistics (by reducing the background uncertainty arising from \sqrt{n} errors and from galaxy clustering) or using a more restricted background region to reduce the contamination of background counts by real globular clusters.

⁵ There were 394 such images (5% of the total). Visual examination of these showed that 315 were actually two blended objects, 11 were three or more blended objects, 35 were single galaxies, two were globular clusters in N5128 (see § IV), and 31 were apparently single stars. On this basis, the ellipticity criteria were judged to be effective at identifying and separating blended images. While two bright clusters were unfortunately eliminated by this procedure, we expect no faint clusters to be eliminated, because the limits rise toward faint magnitudes.

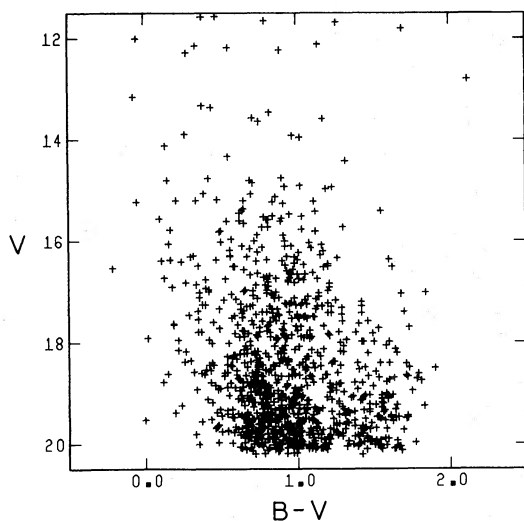


FIG. 3

FIG. 3.—Color-magnitude diagram of 1000 round images.

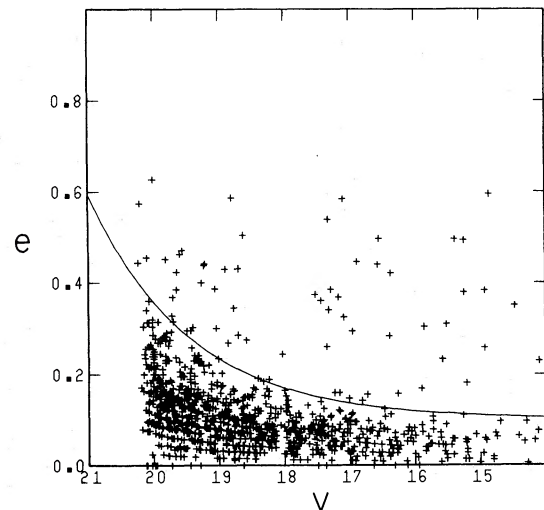


FIG. 4

FIG. 4.—Ellipticities of 1000 images on the V plate. The line shows the limit used to define elliptical images. Most images above the line are blended stars.

The total number of objects detected in each ring, N , and the surface density, σ , are shown in Table 2. The numbers include the 394 elliptical images and an additional 343 objects that were added to correct for the missing blended objects. (These were added at the locations of 86% of the elliptical images, chosen randomly by the computer. This correction accounts for the numbers of single, double, and triple objects that were found visually and noted above.) The background surface density found in the outer seven rings is $5.21 \pm 0.08 \text{ arcmin}^{-2}$. The number of excess objects over background in the inner fifteen rings is then found to be 164 ± 91 , where the error is estimated from the \sqrt{n} errors in both the counted objects and the background. If the distribution of globular clusters follows the halo light (an $r^{1/4}$ law with $r_e = 5.5$ [van den Bergh 1976]), then the background counts are contaminated by about 25 objects. Correcting the background surface density to 5.18 ± 0.08 gives 188 ± 91 excess objects in the inner rings. This correction to the background requires extrapolating the cluster distribution to $r = 22'$, well beyond the radius $r \sim 10'$ where the halo light has been measured. Therefore, the error in the correction may be as much as the correction itself, but it is probably not much larger. If the clusters follow the halo light at all radii, then we find that 61% lie in the counted region (including 7% that lie in the region we used to estimate the background), 23% lie inside the counted region, and 16% lie outside.

From these numbers, the total number of globular clusters in N5128 above the plate limit can be estimated. The results are shown in Table 3 for all detected objects, as just described, as well as for limited ranges of magnitude, for the case of excluding all elliptical images, and for the case of excluding very blue and very red objects. The limits for these ranges were chosen conservatively so as not to exclude appreciable numbers of clusters. The best estimate for the number of clusters in the counted region brighter than $V = 19$ is 55 ± 58 , and brighter than $V = 20$ it is 209 ± 80 . In order to compare with the slightly larger region (4.5–52.0 mm) counted by HHHC, these numbers should be scaled up by a factor 1.10, to 61 ± 64 and

TABLE 2
IMAGE COUNTS FOR ALL IMAGES DETECTED

Ring Size (mm)	$\langle r \rangle$ (arcmin)	Area (arcmin ²)	N	σ (arcmin ⁻²)
6–9	2.28	5.4	34	6.35 ± 1.09
9–12	3.22	11.6	57	4.90 ± 0.65
12–15	4.16	17.2	119	6.90 ± 0.63
15–18	5.09	22.8	140	6.15 ± 0.52
18–21	6.02	28.3	160	5.66 ± 0.45
21–24	6.96	33.7	179	5.31 ± 0.40
24–27	7.89	46.2	276	5.98 ± 0.36
27–30	8.82	51.6	254	4.93 ± 0.31
30–33	9.75	57.0	305	5.35 ± 0.31
33–36	10.68	62.4	338	5.41 ± 0.29
36–39	11.61	67.9	386	5.69 ± 0.29
39–42	12.54	73.3	353	4.82 ± 0.26
42–45	13.47	78.7	442	5.62 ± 0.27
45–48	14.40	84.1	418	4.97 ± 0.24
48–51	15.33	89.6	478	5.34 ± 0.24
51–54	16.26	95.0	477	5.02 ± 0.23
54–57	17.19	100.4	521	5.19 ± 0.23
57–60	18.12	105.9	578	5.46 ± 0.23
60–63	19.05	111.3	607	5.45 ± 0.22
63–66	19.98	116.7	597	5.12 ± 0.21
66–69	20.91	122.2	630	5.16 ± 0.21
69–72	21.84	127.5	651	5.10 ± 0.20

TABLE 3
NUMBER OF GLOBULAR CLUSTERS DETECTED

Object	Detected 6 to 51 mm	After Correction to Background	Extrapolated Total for Galaxy
All objects detected:	164 ± 91	188 ± 91	349 ± 168
$16.5 \leq V \leq 18.0$	1 ± 39	1 ± 39	2 ± 72
$16.5 \leq V \leq 19.0$	48 ± 58	55 ± 58	102 ± 108
$16.5 \leq V \leq 20.0$	183 ± 80	209 ± 80	388 ± 148
Only round images	122 ± 86	141 ± 86	262 ± 160
Only $0.3 \leq B - V \leq 1.3$	97 ± 72^a	122 ± 72^a	375 ± 222

^a Region restricted to 15–51 mm, to avoid color errors near center of N5128.

231 ± 88 . The comparison is done by HHHC, where good agreement is found between the cluster luminosity function in N5128 and that in Local Group galaxies over a range of 5.2 magnitudes.

IV. SIZES OF THE GLOBULAR CLUSTERS

The largest globular clusters in N5128 are resolved on our plates. Their slightly extended images allowed HHHB to identify 24 as nonstellar, probable clusters, of which 17 were observed spectroscopically and confirmed as member clusters in N5128. Estimates were also made by HHHB of the sizes of the confirmed clusters. The extended nature of the largest clusters also allows them to be distinguished with the COSMOS data: nonstellar images have larger areas for their magnitude than stellar images. The COSMOS data allow us for the first time to make objective estimates of the sizes of all of the clusters in N5128.

a) A New Sample of Cluster Candidates

As an example of our data, 1000 images from the V plate are plotted in Figure 5a. Most elliptical images are close, blended objects, and some are background galaxies, but very few are globular clusters (§ III and below), so eliminating them does not bias the analysis of the cluster sizes. (Because the limits that define elliptical images rise toward faint magnitudes, no faint clusters should be eliminated because of ellipticity.) The round, extended images remaining above the stellar sequence should include background galaxies, a few plate flaws, and nearly all of the largest globular clusters.

We have fitted lines by eye to the stellar sequences in Figure 5a and the corresponding figures for the other plates. For each image, a residual from the line was found for each plate and a mean residual, δA , was computed. The J and F plates could not be used inside radii of 30 and 21 mm, respectively, because of incomplete background subtraction of the halo light. Also, the B plate showed a considerably larger scatter in the stellar sequence at all radii (for unknown reasons), so it was not used at all. We made various tests for systematic errors that might affect δA , using each plate individually and their combination. Three examples are shown in Figure 6, where δA (the mean residual for the three plates) is plotted for 1000 round images lying in a north-south strip through the center of N5128.

In the full area studied, there were 260 images with $\delta A > 4$ pixels and $V > 16$, but 41 of these had a large residual on only one plate, due to a plate flaw or crowding. The remaining 219 images constitute a complete, automatically selected sample of extended images that we hoped would contain many globular clusters. However, we expected some contamination from galaxies and blends after distilling the very large initial data set, so

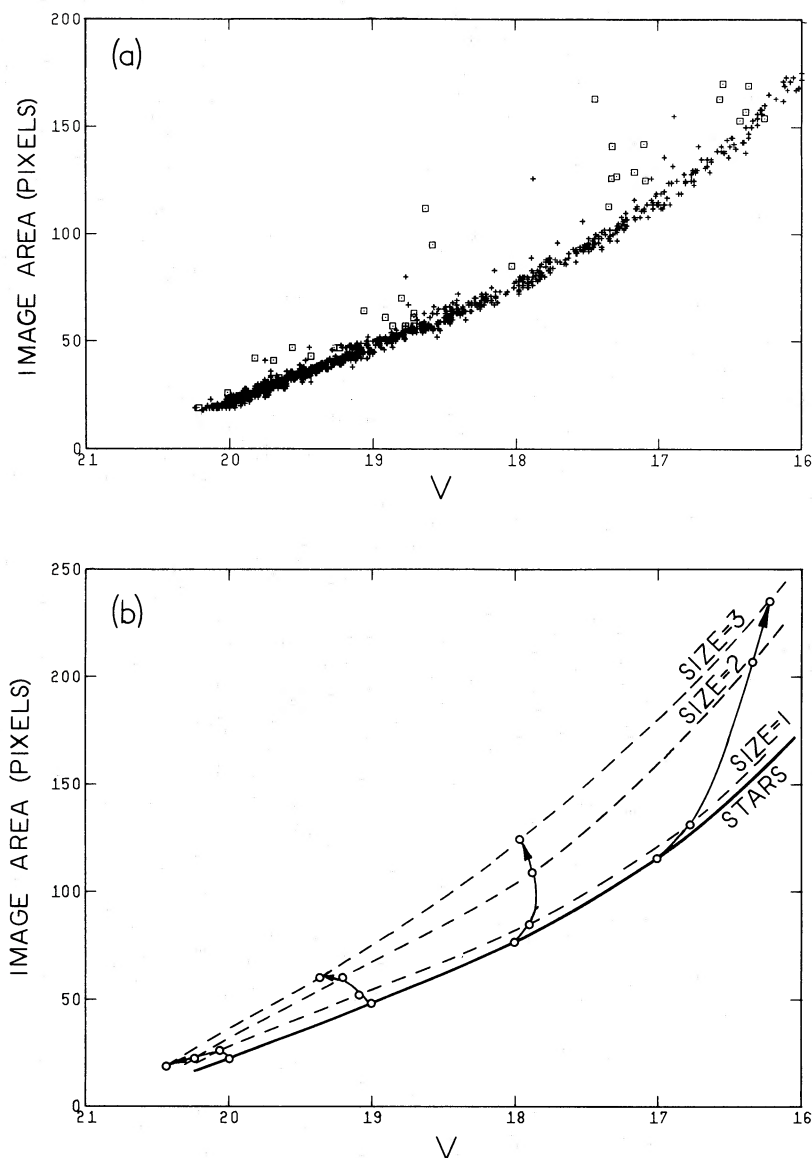


FIG. 5.—Areas of images measured on the V plate. In (a), 1000 images have been plotted, with those found to be elliptical plotted as squares. Of the remaining round images lying above the stellar sequence, many are globular clusters. In (b), model globular clusters are plotted. The arrows show how clusters change in measured (isophotal) magnitude and area on the V plate as they become more extended. “Size = 1” clusters have core radii of $5 \mu\text{m}$ and tidal radii of $150 \mu\text{m}$ (1.5 pc and 45 pc if $D = 3.3 \text{ Mpc}$). Clusters larger than this should be identifiable on our plates.

we then supplemented the automatic processing with manual visual inspection.

All extended images were examined visually (by each of us independently and without reference to any previous classifications) to try to assess the composition of the sample. Grades were assigned to indicate the probability that an object might be a globular cluster by trying to judge whether the image was, in fact, nonstellar and whether it had the very diffuse or structured appearance of a background galaxy. The distribution of grades is shown in Figure 7. Several facts quickly became clear: among the brightest objects ($16 < V < 18$), approximately half are stars whose images are distorted by coma near the perimeter of our field, or sometimes by fainter blended images (bright objects with poor grades in Fig. 7); a few obvious galaxies remain in our sample at all magnitudes, with the number increasing toward fainter magni-

tudes; our visual image classification is not very reliable for faint images ($V > 19$), and cannot give us convincing information about their nature.⁶

Manual searches made from 1980 to 1983 had already identified as possible clusters many of the COSMOS sample objects. Correlation of the several independent manual searches and the COSMOS search shows that no single search, manual or automatic, has been very complete. Even repeated

⁶ It is possible that the visual search techniques could be improved at fainter magnitudes. HBBH noted that the nonstellar nature of images was more difficult to evaluate on III-a emulsions than on II-a. Furthermore, the overwhelming majority of the II-a plates searched have been optimally exposed for the (stellar) magnitude range 17–19. Improved reliability at magnitudes $V > 19$ would presumably result from any of the following: (1) deeper exposures on II-a emulsions, (2) improved seeing (and/or optics in the camera), and (3) higher plate scale.

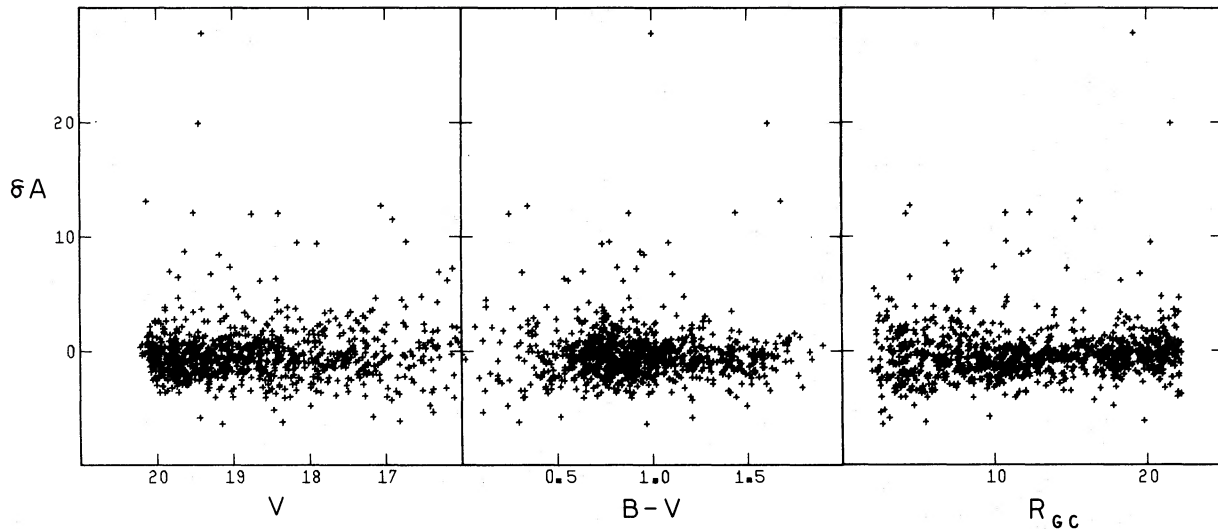


FIG. 6.—Residual areas of 1000 round images plotted against magnitude, color, and distance from N5128 (in arcmin)

classifications by the same person using the same plate frequently disagree, showing the subtlety of the nonstellar character of the clusters. On our plates, the uncertainty is greatest for faint objects, suggesting that the average classification given by several of us is more likely to be useful at all magnitudes. Therefore, we have taken all the extended objects graded as having at least a “fair” probability of being clusters to be a new sample of cluster candidates. There are 79 objects in the new sample.

The COSMOS search produced only a few new, bright candidates with high visual grades, and none were very extended. (There were 14 new candidates with $V < 19$, and the most extended had $\delta A = 13$ pixels.) This result indicates that the combination of several searches to date has probably identified almost all of the brightest, most extended clusters. HHHB suspected this result was true for their earlier searches, but could not argue quantitatively. Most of the new, likely candi-

dates found in the COSMOS search are faint and/or only slightly nonstellar. The completeness of the COSMOS search is discussed further in § IVc. The criteria used to select extended objects from the COSMOS data have resulted in recovery of 17 of the 27 clusters and likely candidates already published (HHBH). Of the 10 not recovered, five were rejected as being elliptical or blended (including cluster No. 1, which is obviously elliptical), four were not found to be sufficiently extended, and one lies outside the COSMOS analysis region.

b) Model Clusters

The actual sizes of clusters can be estimated by comparison of the data to a model. We constructed a model of the COSMOS data as follows. Model star images with a wide range of magnitudes were generated and “measured” by our “model COSMOS” (i.e., the COSMOS measuring algorithm was applied) using the intensity threshold for each pixel and the area threshold for each image actually used for each plate. Using the known transmission-intensity relation and values of background transmission and saturation transmission found by COSMOS for each plate, we inferred the point spread function for each plate by forcing the model area-magnitude and COSMAG-magnitude curves to agree with the real measured curves. (We could not achieve a perfect match to both measured curves, probably because the COSMOS transmissions are affected by the spot halo in a way that makes the transmission-intensity relation slightly different for the sensitometer spots than for the real star images, but we feel the match was adequate.) We then generated model star images with noise, taking values of plate noise for II-a and III-a emulsions from Latham (1978) and COSMOS measuring noise from Stobie (1982), and “measured” them with the COSMOS algorithm. The dispersion in the model area-magnitude, COSMAG-magnitude, and ellipticity-magnitude relations agreed very well with the behavior of the real measured relations for each plate. This agreement gave us confidence that the model actually reproduces the photographic-scanner system quite realistically. Finally, model cluster images with various total integrated magnitudes were generated, convolved with the same point spread function used for stars, and “measured” in the same way.

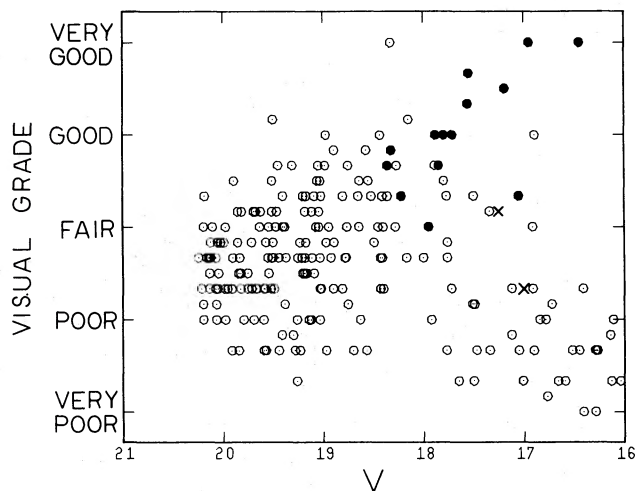


FIG. 7.—Grades showing the likelihood that an object is a globular cluster, based on visual examination of the extended images found by COSMOS. Confirmed clusters (from radial velocities; see HHHB) are shown by filled circles, and confirmed stars by crosses. Objects in the lower right are mostly stars, and many faint objects are background galaxies.

The behavior of model clusters on the V plate is shown in Figure 5b, and the behavior on the other plates is very similar. Clusters with total magnitudes of $V = 17, 18, 19,$ and 20 are shown. The behavior is surprisingly complicated because of the combined effects of saturation and an isophotal threshold: as a bright cluster becomes increasingly extended, it is measured to be brighter and bigger as its image area (mostly saturated pixels) grows; however, a faint cluster is measured to be fainter as more of its light falls outside of the threshold isophote. Each plate reacts slightly differently; therefore the magnitudes and colors measured by COSMOS can be in error by as much as 0.6 and 0.2 mag, respectively, for the bright, most extended clusters.

The model clusters all have King-model profiles (King 1962). Those in Figure 5b have $r_t/r_c = 30$. The first line of clusters has $r_c = 5 \mu\text{m}$ and $r_t = 150 \mu\text{m}$ ($0''.09$ and $2''.8$, respectively, corresponding to 1.5 pc and 45 pc, respectively, at a distance of 3.3 Mpc [see HHBH]), and the others have sizes twice and three times as large. Model clusters with different concentrations (from $r_t/r_c = 6-100$) were also run, and the results are similar to Figure 5b: the COSMOS parameters are sensitive to a combination of r_c and r_t , but we cannot distinguish the two. The model shows that the clusters with Size = 1 in Figure 5 should have residual areas on the V plate from 3 to 10 pixels (in the absence of noise) and should often be distinguishable; clusters 40% larger than Size = 1 should be distinguishable at all magnitudes to $V = 20$ on our plates.

c) Discussion

The distribution around N5128 of the extended objects with high visual grades from the COSMOS search is shown in Figure 8. There is a weak concentration toward the center of N5128, but it is disappointingly weak. A combination of effects probably masks the stronger concentration indicated by the star counts for the entire system: clusters toward the center of N5128 are smaller (HHBH), so are discriminated against in the COSMOS sample; at least some contamination of the sample by stars and galaxies is still occurring; the brightest clusters may, in fact, be more widely distributed than the fainter ones that dominate the star counts. We discuss these effects further in the remainder of this section.

The extension (the residual, δA , from the stellar area-magnitude sequence) of all the likely candidates from the

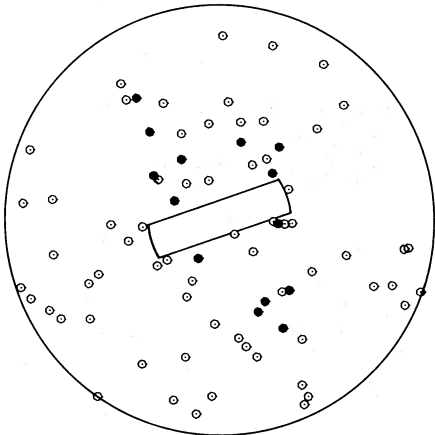


FIG. 8.—Distribution on the sky of all likely cluster candidates found by COSMOS. Confirmed clusters are shown by filled circles.

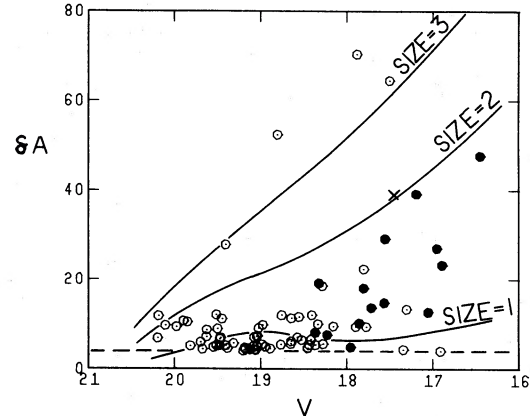


FIG. 9.—Residual areas of all likely cluster candidates found by COSMOS (residuals from the stellar sequence at $\delta A = 0$). Confirmed clusters are shown by filled circles. The solid lines show the extension of model clusters as in Fig. 5. The dashed line shows the sample threshold. A model of ω Cen at a distance of 3.3 Mpc is shown by the cross (\times).

COSMOS search is shown in Figure 9. The extension of model clusters is also shown, including a model corresponding to ω Cen. (In our Galaxy, ω Cen is the most luminous cluster and one of the largest. The model is a spherical King model with $r_t = 270 \mu\text{m}$, $r_c = 12 \mu\text{m}$, $V = 17.76$, corresponding to ω Cen at a distance of 3.3 Mpc.) Figure 9 indicates that the large size of ω Cen is not extreme when compared with the clusters of similar luminosity in N5128, confirming the earlier evidence and extensive discussion by HHBH based on visually identified clusters.

The size distribution of COSMOS images provides a way to investigate the sample completeness more fully than could be done by HHBH. Of the brightest cluster candidates in Figure 9, most are sufficiently extended to be easily identified from our data. Four facts indicate that the discovery of clusters brighter than $V \sim 18$ is reasonably complete within the area of our analysis. (1) Few bright, marginally extended candidates (near the $\delta A = 4$ threshold) are seen in Figure 9. The distribution for bright clusters contrasts with that for fainter clusters, and suggests that no large population of bright, compact clusters lies below our threshold. (2) Spectra of a few bright, marginal candidates taken in 1983 showed that most were foreground stars. (3) We noted above that the recovery statistics suggest we have found most of the bright, extended objects. Finally, (4) the image counts in Table 3 do not show a large number of excess bright objects (although the statistical errors are large for $V < 18$). Admittedly, a few bright, compact clusters are almost certainly escaping identification. (An example is cluster No. 23, found in the sample-B spectroscopic search of HHBH, which is bright but sufficiently compact to have escaped identification in all the searches for extended objects.) Nevertheless, we believe that these observations indicate that the bright tail of the luminosity function in N5128 is now known quite well, probably to within a factor of 2.

We can also see in Figure 9 that a large fraction of the brightest cluster candidates are very extended. Several are comparable to ω Cen in size, and two others not in the COSMOS sample (numbers 1 and 16) are probably larger, as discussed by HHBH. (The comparison assumes $D = 3.3$ Mpc for N5128, as argued by HHC; if the distance is larger, then the sizes are proportionally larger.) In contrast, most of the candidates fainter than $V \sim 18$ are probably more compact.

The distribution of δA in Figure 9 suggests that numerous faint, more compact clusters exist in N5128 but have not exceeded the $\delta A \geq 4$ pixel limit defining extended objects. The image counts in Table 3 support this idea: about 50 excess objects were found in the counted area with $18 < V < 19$, and about 150 with $19 < V < 20$. Therefore, the sample of extended images is increasingly incomplete at these magnitudes. Again, the recovery statistics for extended images are good, so most of the missing clusters are probably compact.

The magnitudes of the cluster candidates are shown in Figure 10, plotted against the distance from the center of N5128. A trend is apparent such that outlying candidates are systematically fainter. This trend was also noted by HHBH among their confirmed and candidate cluster (see their Fig. 6). HHBH suggested that a combination of a selection effect and a real astrophysical effect was the cause of the apparent trend. The same effects are probably responsible for the apparent trend in the COSMOS-selected sample in Figure 10: faint, compact clusters are selected against in both the manual search of HHBH and the automatic search here (because a faint cluster has to be larger than a bright cluster if it is to exceed the threshold of the eye or COSMOS), and compact clusters lie systematically closer to the center of N5128. The latter statement is true for bright clusters in N5128 (HHBH), it is true for all clusters in our Galaxy, and it has some physical explanation in tidal effects, so it is probably also true for faint clusters in N5128. The result is to leave the lower left corner more incomplete than any other part of Figure 10. Furthermore, this effect may be the dominant reason that the cluster candidates in Figure 8 do not show a stronger concentration toward N5128.

If the clusters in N5128 have values of M/L similar to clusters in our Galaxy, then, for the same luminosity and perigalactic distance, they should have tidal radii *smaller* by about a factor of 1.5. (This conclusion is based on the mass of N5128 found by HHBH being larger than the mass within the same radius in our Galaxy by about a factor of 3, and $r_t \propto M_G^{-1/3}$.) However, the most luminous clusters in N5128 (at $V \sim 17$) should have about 3 times *larger* tidal radii than those at the peak of the luminosity function (based upon assuming that M/L does not depend on L , $r_t \propto M_{cl}^{1/3}$, and $D = 3.3$ Mpc). The increasing extension of the bright candidates seen in Figure 9 is consistent with this expected increase in their tidal radii. We do

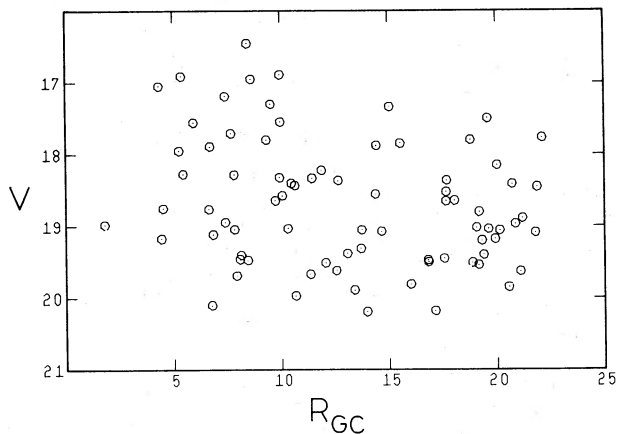


FIG. 10.—Magnitudes of likely cluster candidates plotted against distance from N5128 (in arcmin).

not know how the core radii of very luminous clusters should behave; the core radii of the bright clusters in N5128 may also be large like that of ω Cen and contribute to the extension in Figure 9, but our data cannot confirm this. The sizes of the fainter candidates in Figure 9 are entirely consistent with their being part of a population of clusters having a size distribution similar to clusters in our Galaxy. The tendency for the brightest clusters to be larger than fainter clusters is also found among M31 by Buonanno *et al.* (1982), although Crampton *et al.* (1984) suggest that the core radii of M31 clusters may behave differently.

Finally, we have compared the positions of the confirmed clusters and cluster candidates with the HRI X-ray image from Figure 2a of Feigelson *et al.* (1981). The X-ray image shows possible (marginally detected) sources in the halo of N5128 with X-ray luminosities of $\sim 10^{38}$ ergs s^{-1} (for $D = 3.3$ Mpc). The most X-ray luminous cluster in M31 emits 10^{38} ergs s^{-1} , so we might expect some of the clusters in N5128's larger cluster system to be detected. On the other hand, the X-ray clusters in the Galaxy and M31 are systematically the most compact clusters, while our identified clusters and candidates are systematically the least compact in N5128 and so are probably not likely to be X-ray sources. In fact, no detections more frequent than expected by chance are seen.

V. CONCLUSIONS

The use of automated techniques to search for globular clusters in N5128 has proven to be difficult but feasible. Distinguishing clusters from *both* foreground stars and background galaxies is a more challenging task than just separating stars from galaxies, whether it is done automatically or by visual inspection of the plates. Although visual inspection has been extremely effective in the exploratory work on N5128 clusters (HHBH), our experience with these manual searches in N5128 indicates to us that they cannot be relied on for completeness within several magnitudes of the plate limit, and, even for brighter images, classifications are not always repeatable. Automated searches are limited by a different problem: in searching a large field for a few special objects (as in the N5128 case), the misclassification of even a small fraction of images (pathological cases such as blended triple stars, a star plus galaxy, a plate flaw, etc.) can seriously contaminate the results. Supplementing an automated search with a visual examination is an efficient way to minimize this problem. Carrying out this procedure in N5128 has recovered most of the bright clusters and good candidates found earlier, it has found some good new candidates at bright and intermediate magnitudes, and it has identified many faint objects as likely candidates.

Perhaps more important than the efficiency of an automated search are the objectivity and the possibility of deriving quantitative measures of the search limits. Two important results have come from the new search in N5128. (1) The failure to find many bright ($V < 18$), compact cluster candidates suggests that most of the bright clusters in N5128 have already been found, and that the bright tail of the luminosity function is now fairly well known. Our spectroscopic confirmation of many individual clusters in N5128 sets a firm lower limit, and our arguments (in § IVc) concerning completeness suggest a close upper limit. The bright end of the luminosity function determined in this way is not subject to the statistical uncertainties of counting excess images above background, as must be done at present for Virgo Cluster galaxies. Furthermore, the brightest confirmed clusters and candidates tend to be quite large

(probably, at least partly, because of their expected large tidal radii). If the sample of bright clusters is indeed largely complete, then this tendency must be real, and does not arise from selection of only the largest clusters. (2) The presence of many faint compact cluster candidates agrees with the number of excess images from the image counts, and the data on their sizes are consistent with their having a similar size distribution as the clusters in our Galaxy.

The COSMOS scanner and reduction process has proven to be effective for this project. Its advantages—high scanning speed and efficient software to process the large data arrays and to detect images—allowed the scanning and detection parts of the project to be finished quickly. Two disadvantages have probably limited the results, however. The reduction of each image to only a few parameters probably constitutes an oversimplification and leads to a loss of information, while a more sophisticated analysis (to try to process blended images, for example) might be worthwhile. Second, the limited dynamic

range of the transmission values recorded by the scanner loses information at high densities (particularly on the III-a plates) that would be useful in identifying nonstellar images. The rapid saturation of images combined with the nonstellar nature of some images complicates the analysis; the effects were surprising, and a model was needed to understand them. Recent improvements to both the COSMOS hardware and software will reduce these disadvantages in future work, and should make it even more effective for projects of this nature.

We are most grateful to R. Humphreys and D. McElroy for lending us three high-quality plates, and to W. Harris and S. van den Bergh for helpful discussions and encouragement. This work was largely supported by the Natural Sciences and Engineering Research Council of Canada, through a grant to W. Harris. G. L. H. H. also acknowledges the support of a grant from the Natural Sciences and Engineering Research Council of Canada.

REFERENCES

- Buonanno, R., Corsi, C. E., Battistini, P., Bonoli, F., and Fusi Pecci, F. 1982, *Astr. Ap. Suppl.*, **47**, 451.
 Chiu, L.-T. G. 1976, *Pub. A.S.P.*, **88**, 803.
 Crampton, D., Schade, D., Chayer, P., and Cowley, A. P. 1984, preprint.
 Ebnetner, K., and Balick, B. 1983, *Pub. A.S.P.*, **95**, 675.
 Feigelson, E. D., Schreier, E. J., Delvaille, J. P., Giacconi, R., Grindlay, J. E., and Lightman, A. P. 1981, *Ap. J.*, **251**, 31.
 Frogel, J. A. 1984, *Ap. J.*, **278**, 119.
 Graham, J. A. 1981, *Pub. A.S.P.*, **93**, 291.
 Graham, J. A., and Phillips, M. M. 1980, *Ap. J. (Letters)*, **239**, L97.
 Hanes, D. A. 1977, *M.N.R.A.S.*, **180**, 309.
 Harris, G. L. H., Hesser, J. E., Harris, H. C., and Curry, P. J. 1984, *Ap. J.*, **287**, Dec. 1984, in press (HHHC).
 Harris, W. E. 1983, *Pub. A.S.P.*, **95**, 406.
 Harris, W. E., and van den Bergh, S. 1981, *A.J.*, **86**, 1627.
 Hesser, J. E., Harris, H. C., van den Bergh, S., and Harris, G. L. H. 1984, *Ap. J.*, **276**, 491 (HHBH).
 Jarvis, J. F., and Tyson, T. A. 1981, *A.J.*, **86**, 476.
 King, I. 1962, *A.J.*, **67**, 471.
 Latham, D. W. 1978, AAS Photobulletin No. 18, p. 3.
 McElroy, D. B., and Humphreys, R. M. 1982, *Pub. A.S.P.*, **94**, 828.
 Stobie, R. S. 1982, *COSMOS User Manual* (Royal Observatory Edinburgh).
 Tubbs, A. D. 1980, *Ap. J.*, **241**, 969.
 van den Bergh, S. 1976, *Ap. J.*, **208**, 673.
 van den Bergh, S., Hesser, J. E., and Harris, G. L. H. 1981, *A.J.*, **86**, 24 (BHH).

G. L. H. HARRIS: Physics Department, University of Waterloo, Waterloo, ON N2L 3G1, Canada

H. C. HARRIS and J. E. HESSER: Dominion Astrophysical Observatory, 5071 W. Saanich Rd., Victoria, B.C. V8X 4M1, Canada

H. T. MACGILLIVRAY: Royal Observatory, Blackford Hill, Edinburgh, EH9 3HJ, Scotland, UK